Available online at www.sciencedirect.com
ScienceDirect
Trans. Nonferrous Met. Soc. China 33(2023) 3476−3486
Transactions of Nonferrous Metals Society of China
www.tnmsc.cn

Hydrothermal activity and metallogenic environment revealed by seismic wave tomography in Yunnan Province, China

Ya SUN[1,2], Shi-lin DENG[1,2], Jian-xin LIU[1,2], Syed Muzyan SHAHZAD[1,2], Bo CHEN[1,2]

1. School of Geosciences and Info-physics, Central South University, Changsha 410083, China;
2. Hunan Key Laboratory of Non-ferrous Resources and Geological Hazard Detection, Central South University, Changsha 410083, China

Received 3 March 2023; accepted 21 September 2023

Abstract: S-wave velocity structures are revealed using double-difference tomography, which shows large-scale low-velocity anomalies around the Xiaojiang and Lijiang−Xiaojinhe fault zones at 10−25 km depth. In contrast, an obvious high-speed anomaly exists in the center of Emeishan area, which is consistent with the Emeishan Large Igneous province. Combined with the geological and geophysical data, the low-velocity anomaly might relate to the lower crustal flow of central Tibetan Plateau. The high-velocity anomaly associated with mantle plume in Emeishan would obstruct the crustal flow and limit it around the large deep faults. Meanwhile, the results also show that many mineral resources are mainly concentrated on the major faults and low-velocity zones, indicating that the lower crustal flow and the large deep faults provide conditions for mineral fluids and minerals deposit.

Key words: Yunnan Province; seismic wave tomography; lower crustal flow; metallogenic environment

1 Introduction

Yunnan Province, China, located on the southeastern margin of the Tibetan Plateau, had experienced the compressive stress associated with the subduction of the Indian Plate. Due to the continuous collision between the Indian and Eurasian plates, the crustal thickness had doubled, and the surface of the Tibetan Plateau was uplifted, becoming the highest Plateau in the world. Due to the tectonic activity, metamorphic and igneous rocks, including gneiss, schist, and granites, were exposed in the Yunnan Province [1−3]. The lower crustal flow and weak lower crust were generally considered the popular dynamic models in the southeastern margin of the Tibetan Plateau [4−6]. Yunnan Province, as a necessary passage for the crustal flow, is the most critical area for heat and mass exchange. It provides a window to constrain the spatiotemporal evolution of the crust and the related tectonic thermal activities for the mineral system. Therefore, the detailed structure of the crust, especially the magmatism and fluid associated with large deposits and ore groups, is of great significance for further understanding the distribution of mineral deposits and the deep dynamic process of deposit formation.

Seismic imaging was a powerful tool for exploring the earth's subsurface. It could identify mineral deposits and reveal the presence of mineral-rich layers [7]. Seismic imaging was also used to detect copper, gold, lead and zinc deposits in the Yunnan Province [8]. Various mineral deposits, including copper, lead, zinc, and gold, were widely spread along the main faults in the Yunnan Province [7−9]. Most of the mineral deposits in this area were mainly formed during the Mesozoic and Cenozoic eras [10,11], which might relate to the magmatic events and heat gradient flow associated

Corresponding author: Bo CHEN, Tel: +86-18570078316, E-mail: bochen@csu.edu.cn
DOI: 10.1016/S1003-6326(23)66348-4

with the collision of the Indian and Eurasian plates [8,12]. Seismic tomography shows that the low-velocity anomalies correlate well with the main faults and the range of metallic minerals in this area [13,14], suggesting that the velocity anomalies might be responsible for forming metallic minerals in the Yunnan Province. Thus, the crustal structure revealed by seismic tomography can provide important information for crustal deformation and deep metallogenic environment.

In this study, we applied the high-resolution double-difference tomography to obtain a detailed shear wave velocity structure of the crust in Yunnan Province (Fig. 1) based on the direct-S wave arrival time. We further compare these results with the active faults, crustal deformation, and magmatic events. The relationships between the velocity anomalies in the crust and the mafic rocks in Yunnan Province and its surroundings are further discussed in this paper. Our results can play a vital role in building the crust structure and its relation to Cenozoic mineralization associated with heat flux and volatiles from the lower crust to the asthenosphere in Yunnan Province and its surroundings.

2 Data and method

2.1 Data

Eighty-two seismic stations are applied in the double-difference tomography in the region of E98°−106° and N22°−28° (Fig. 1) recorded by the China Earthquake Administration (CEA) network [15]. The direct S-wave travel time generated by 17331 earthquakes is collected with a magnitude larger than 1.0 between January 2009 and December 2020 (https://data.earthquake.cn) in Yunnan Province and its surroundings. The outliers of S-wave arrival time are further deleted to improve the inversion resolution by selecting the phase data with uncertainties less than ±5 s relative to the travel time curves (Fig. 2). Meanwhile, the selected events are recorded at least eight stations and the distance of the station-pair should be larger than 10 km. Finally, 138565 direct S-wave travel time is obtained in this work. 124445 differential event pairs are also constructed based on these catalog travel time. All those S-wave travel time and the event pairs provide good ray coverage and cross-

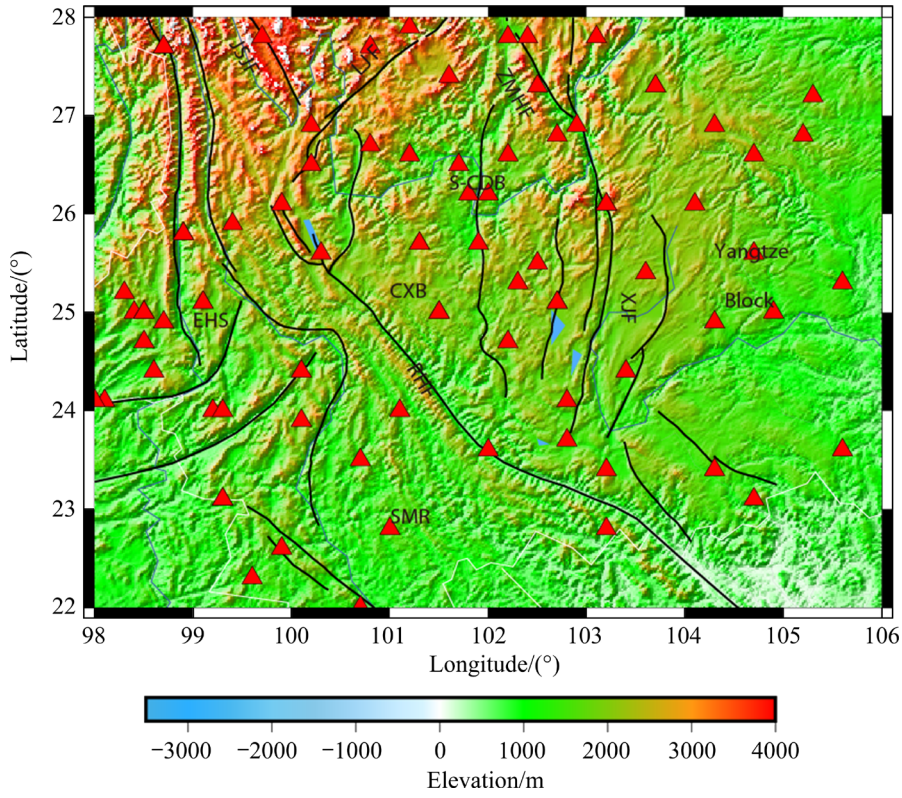

Fig. 1 Topographic map and geological structure of Yunnan Province and its surrounding areas (Red triangle represents the national seismic stations; S−CDB: Southern Chuandian block; CXB: Chuxiong Basin; EHS: East Himalayan syntaxis; SMR: Simao region; JSJF: Jinshajiang fault; LJF: Lijiang fault; ZMHF: Zemuhe fault; XJF: Xiaojiang fault; RRF: Red River fault)

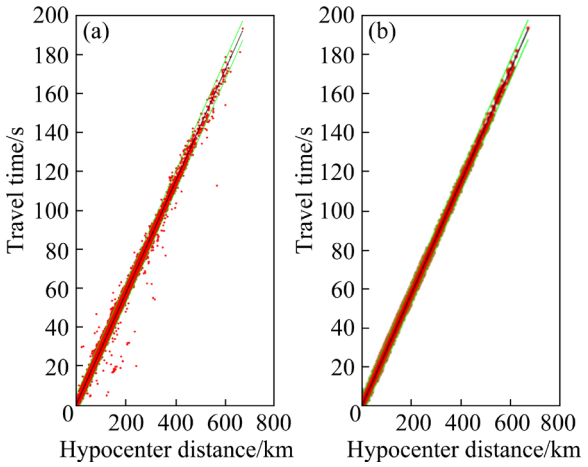

Fig. 2 S-wave travel time before (a) and after (b) filtering

correlation for a reliable double-difference tomography.

2.2 Method

The S-wave travel time t is first calculated along the ray path from an event i to a seismic station k using the ray theory:

$$t_k^i = \tau^i + \int_i^k u \mathrm{d}s \tag{1}$$

where u is the slowness, ds is the differential of ray path length, and τ^j is the original time of the event i. Since the relation between travel time and earthquake event is nonlinear, the residual travel time r can be obtained by Taylor expansion from Eq. (1). The double-difference tomography is built based on the residual time between different events using the result of $(r_k^i - r_k^j)^{\mathrm{obs}}$. A similar equation for event j measured from station k is subtracted from the S-wave travel time. The residual time between two events (i, j) at the same station k can be written as follows [16]:

$$\frac{\partial t_k^i}{\partial m}\Delta m^i + \int_i^k \delta u \mathrm{d}s - \frac{\partial t_k^j}{\partial m}\Delta m^j - \int_j^k \delta u \mathrm{d}s = r_k^i - r_k^j \tag{2}$$

where Δm^{ij}(=($\Delta \mathrm{d}x^{ij}$, $\Delta \mathrm{d}y^{ij}$, $\Delta \mathrm{d}z^{ij}$, $\Delta \mathrm{d}\tau^{ij}$)) is the perturbation of two sources. Since the crustal structure of the Yunnan Province has strong heterogeneity in both vertical and horizontal directions, a one-dimensional initial velocity model should be challenging to invert an accurate result. The 3D seismic wave velocity model of SWChinaCVM−1.0 observed by the adjoint inversion from body wave and surface wave [17,18] is considered the initial model for the double-difference tomography. The lateral grid interval 0.5°×0.5° is finally designed, based on the model resolution and regional seismic ray distribution density. The vertical grid notes are set at −5, 0, 1, 3, 5, 6, 8,10, 15, 20, 30, 35, 40 and 50 km.

Figure 3 shows the distribution of residual travel time before and after inversion. The residuals before inversion are distributed between −4 to 4 s, reflecting a specific deviation between the initial and real models. The residuals after inversion are concentrated from −2 to 2 s, indicating that the final velocity model is better than the initial model in fitting the actual observation time.

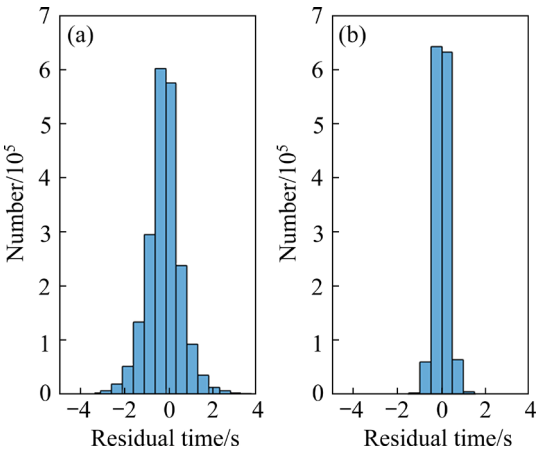

Fig. 3 Histogram of travel time residuals for S-wave before (a) and after (b) inversion

2.3 Checkboard test

The checkboard resolution test was used to evaluate the resolution of seismic velocity models and the ray path coverage [18−21]. The positive and negative perturbations of 5% are added to the initial S-wave model. The synthetic travel time is then measured within the same distribution of station-to-events following the actual data. The checkboard test (Fig. 4) shows that the velocity anomalies can be recovered well from the surface to the depth of 35 km with good ray-path coverage.

3 Results

3.1 Horizontal slices

The horizontal slices in the depths of 0, 5, 10, 15, 20, 25, 30 and 35 km (Fig. 5) show the lateral heterogeneities in the crust. At a shallow depth of 0−15 km, shear wave images show that the Lijiang−Xiaojinhe and the Zemuhe faults located at the boundary of the Chuandian block have apparent low-velocity anomalies. Meanwhile, the velocity

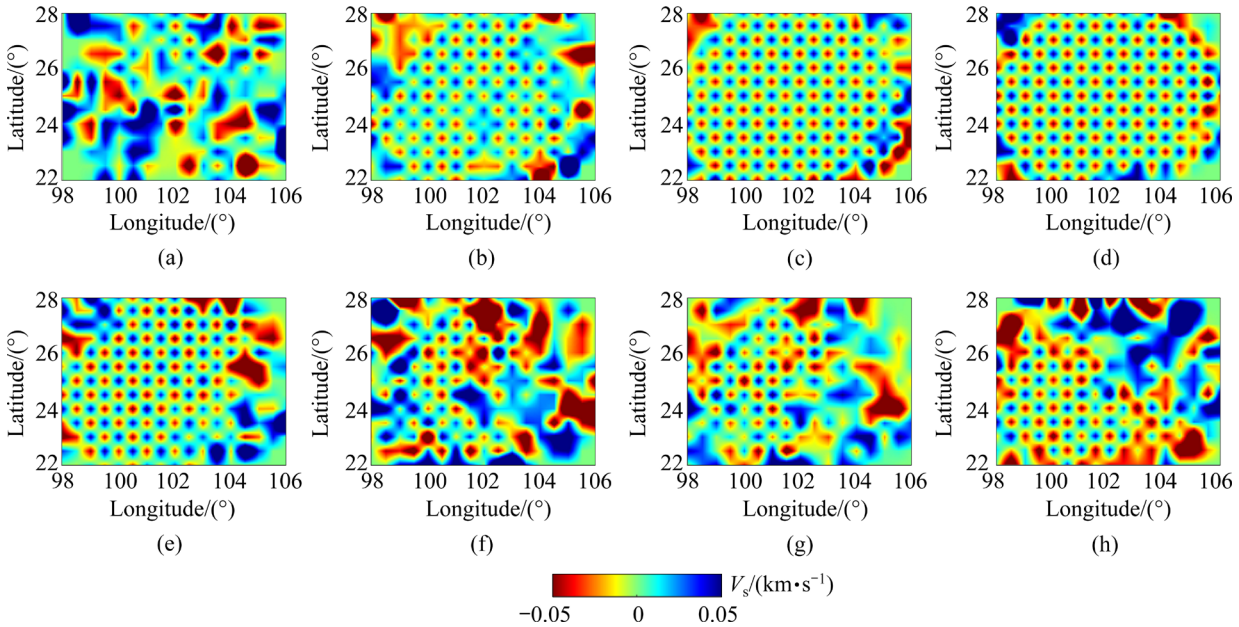

Fig. 4 Checkboard test results for S-wave velocity anomalies at 0 (a), 5 (b), 10 (c), 15 (d), 20 (e), 25 (f), 30 (g), and 35 km (h) depths

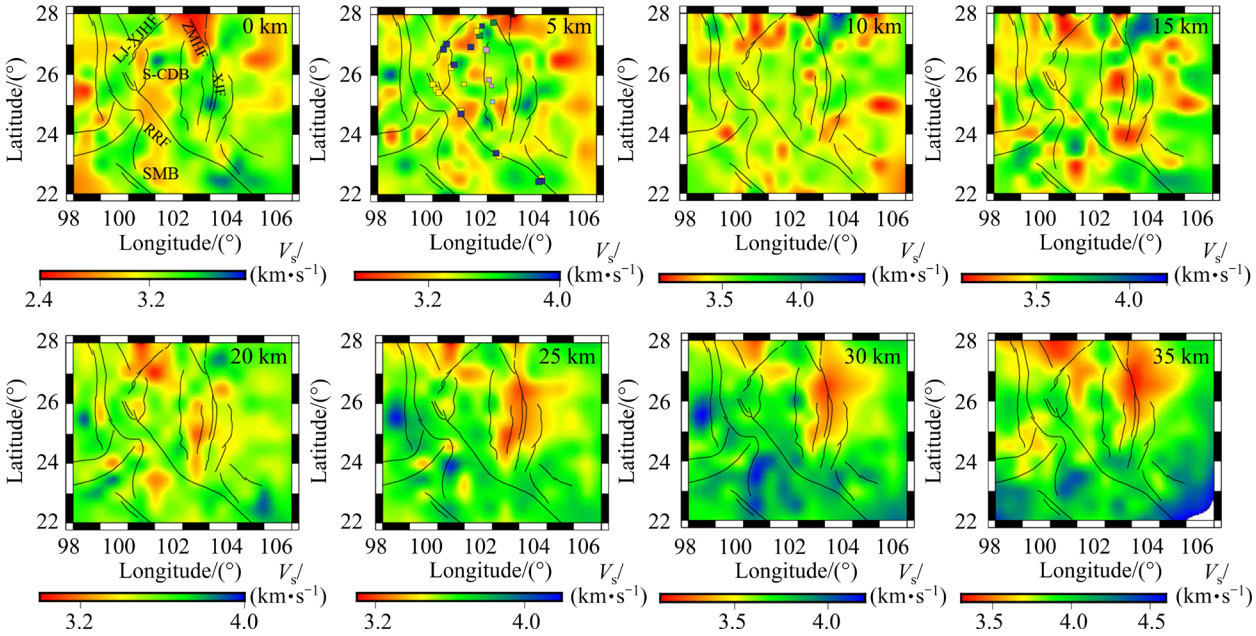

Fig. 5 Horizontal slices of S-wave velocity and mineral deposits (Blue squares represent porphyry (Au−Cu−Mo); yellow squares represent Au deposit; green squares represent carbonatite; cyan squares represent Ni−Cu(−PGE) sulfide deposit; purple represents Fe−Ti−V oxide deposit; LJ−XJHF: Lijiang−Xiaojinhe fault

anomalies are relatively dispersed, indicating that velocity anomalies are mainly influenced by shallow geological structures. At a depth of 15−35 km, the low-velocity anomalies extended from the north Chuandian block to the southwest along the Lijiang−Xiaojinhe fault zone with a belt shape. At the same time, the low-velocity anomaly zone along the Xiaojiang fault zone also appears on the western margin of the Yangtze craton, which is consistent with the surface wave inversion [4]. The columnar high-speed anomalous body is also found in the center of the southern Chuandian block, which extends from the surface to a depth of 30 km. Meanwhile, this high-velocity anomaly extends from the center of Emeishan to the northeast and reaches the Zemuhe fault and the southwest margin

of the Sichuan Basin. In addition, the low-velocity anomalies are centered in the deep large faults, such as the Xiaojiang fault, and Lijiang-Xiaojinhe fault. At a depth of 20−30 km, our inversion shows that the high-velocity anomalies distribute in the Simao and Baoshan blocks.

3.2 Vertical profiles

The vertical profiles of the shear wave velocity along the N24°, N25°, N26°, and E103° are plotted in Fig. 6, which are marked with profiles of *AA′*, *BB′*, *CC′*, and *DD′*, respectively. The profile image of E103° shows that the low-velocity anomalies mainly spread along the Xiaojiang fault with a depth of 15−35 km (*DD′* in Fig. 6). At a depth of 30 km, this low velocity is continuous from the Zemuhe fault to the intersection of the Xiaojiang fault and Red River fault. However, in the shallow depth between 10 and 25 km, the low-velocity anomaly is blocked by a high-velocity anomaly around the center south of the Chuandian block (*BB′*, and *CC′* in Fig. 6). For the vertical seismic profiles of N26° and N25° (*BB′*, and *CC′* in Fig. 6), a significant high-velocity anomaly extends from the center of the southern Chuandian block at about E101−102° to the northeast part. It reaches the southwest part of the Sichuan basin, which separates the low velocity into two parts (*BB′*, *CC′* in Fig. 6). One low-velocity anomaly focuses on the Xiaojiang fault, and the other low-velocity anomaly spreads in the Lijiang−Xiaojinhe fault zone. This high-velocity anomaly is generally considered as the Emeishan Large Igneous province, which is marked by ELIP in Fig. 6 (*BB′*−*DD′*).

4 Discussion

Previous literature [22−24] shows that Yunnan Province is enriched in many mineral deposits, such as gold, silver, copper, and lead−zinc (Fig. 7). These deposits may relate to geothermal activity, forming through hydrothermal fluids and magmatic events in the region. For example, the gold deposits in the Yunnan Province might be caused by intrusions around the active faults. Similarly, the copper deposits might relate to the volcanic rocks in this area [25]. Magmatic events, such as magma intrusion into the crust, can also significantly affect the mineral deposit formation in Yunnan Province [26]. The heat and pressure generated by these events can lead to the formation of mineral deposits [26].

4.1 Main fault and mineral deposits

The horizontal images of the seismic velocity image in our study show large-scale low-velocity anomalies at a depth of 15−35 km, crossing the Xiaojiang fault, the Lijiang−Xiaojinhe, and the northern Red River fault zones (Fig. 5). The Yunnan Province region is known for its rich mineral deposits, and a strong correlation between the location of mineral deposits in Yunnan Province and the presence of certain types of faults and fractures in the subsurface are observed (Fig. 7) [24,25]. Geological data show that many mineral deposits are widely spread around the Lijiang−Xiaojinhe

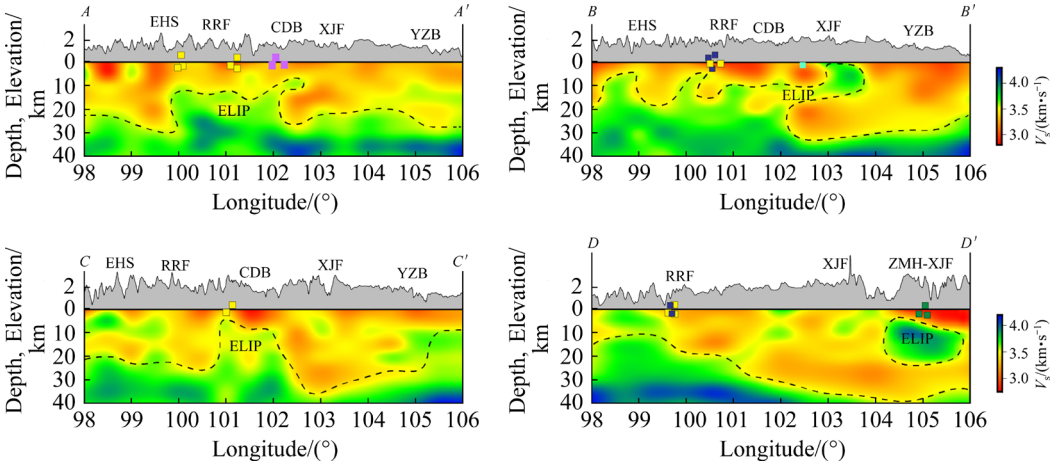

Fig. 6 Vertical profiles along N24° (*AA′*), N25° (*BB′*), N26° (*CC′*), and E103° (*DD′*) for S-wave velocity and mineral deposits (The dashed lines represent the distribution of low speed; the blue and yellow squares represent porphyry (Au−Cu−Mo) and Au deposit, respectively; the green squares, cyan squares, and purple squares represent carbonatite, Ni−Cu(−PGE) deposit, and Fe−Ti−V oxide deposit, respectively)

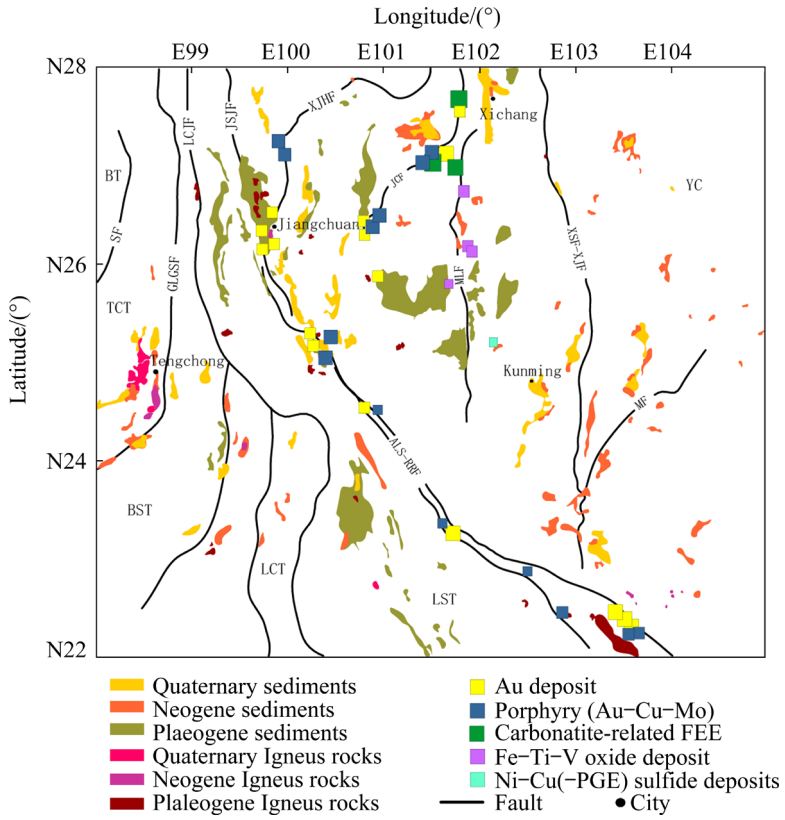

Fig. 7 Distribution map of mineral deposits in Yunnan Province and its surrounding orogens (modified after XU et al [3]) (LT: Lhasa terrane; BT: Burma terrane; TCT: Tengchong terrane; BST: Baoshan terrane; CMSZ: Changning− Menglian suture zone; LCT: Lincang terrane; LST: Lanping−Simao terrane; MF: Milc fault; SF: Shan fault; YC: Yangtze craton; LCJF: Langcangjiang fault; JSJF: Jinshajiang fault; ALS−RRF: Ailaoshan−Red River fault; JCF: Jinhe−Chenghai fault; MLF: Mopanshan−Lvzhijiang fault)

fault and the Zemuhe fault zone with a belt distribution [25], which is consistent with the low-velocity anomaly distribution. The anomalies around the large faults indicate that mineral deposits may be found in these areas, and mineral-rich pockets or veins were formed within the low-velocity anomaly zones [26]. All those observations suggest that the mineral deposition system is linked to the movement of these faults, corresponding to the rotation of the low-velocity anomaly along the Lijiang−Xiaojinhe and northern Red River faults. These also suggest that the distribution of mineral deposits is not uniform, and they only concentrate in specific areas along the large faults.

Magnetotelluric results reveal two high conductivity and low resistance channels at a depth of 20−40 km [27]. One channel distributes along the Eastern Himalaya Syntaxis (EHS), and the other spreads along the Xianshuihe fault and Xiaojiang fault zones. The second channel is consistent with the low-speed zone below the Xiaojiang fault zone, strengthening the link between mineral deposition and fault movement in the Yunnan Province [28,29]. The intense pressure and heat can cause ductile deformation and less resistance to this action at the depth. However, the fault would become inactive when the shear zone cools, which might result in a higher resistivity [30]. The low-resistivity anomalies can reflect this ductile deformation in the crust, which might relate to various factors, such as fluids, partial melting, and sulfide minerals [31]. Furthermore, the low resistivity and low-velocity channels may indicate the presence of mineral-rich fluids in these faults. The minerals in the fluids may deposit minerals as they pass through rock formations. The mineral deposits such as tin, tungsten, and lead−zinc were deposited in the granites along the active faults [31,32]. We argue that active faults play a crucial role in mineral deposit formation in Yunnan Province. The movement of these faults leads to crustal

deformation and rupture of rock layers, creating favorable conditions for mineralization. All those results have shown that mineral deposits such as tin, tungsten, and lead zinc are usually related to active faults in Yunnan Province [32,33]. These faults can cause the uplift and erosion of rock layers, exposing new mineral deposits.

Additionally, the movement of these faults can also cause a change in the existing mineral deposits, leading to the formation of new minerals and metals. Geological data identified that several areas in Yunnan Province have a high potential for gold mineralization based on the presence of active faults and magmatic events [32]. The Dadu River gold deposit is located on the northwest margin of the Yangtze River estuary and has obvious mineralization, which can be traced back to 30−20 Ma. Geological data suggested that this mineralization might relate to the Cenozoic Xiaojiang fault system [33]. A strong correlation between the location of mineral deposits and certain types of faults and fractures in the subsurface was deduced in Yunnan area. Red River fault served as a high-flux conduit of primary magma to collect and release gases, forming multiple gold ore deposits (Ailaoshan gold) at the intersections of faults [34]. The lower crustal flow might exacerbate the activity of faults, resulting in a specific crustal-scale shear zone, which provides conditions for further migration of ore-bearing fluids and ore deposits.

4.2 Emeishan Large Igneous province

The observed high S-wave velocity in the depth of 10−30 km in the Emeishan area is consistent with the distribution of mafic and ultramafic rocks [35,36]. This high-velocity anomaly was generally considered the Emeishan Large Igneous province, marked by ELIP (Figs. 5, 6, *AA′*–*DD′*). The study of peridotite phenocrysts and their inclusions confirms that abundant Neoproterozoic intrusive igneous rocks with granodioritic to mafic–ultramafic compositions are widely distributed in this region [35]. It implies that mineral deposit system in the Yunnan Province is related to the ELIP [37].

The Emeishan basalts exhibit distinct Petro-chemical characteristics, with two main chemical groups (low-titanium and high-titanium). The low-titanium basalts have similar attributes to arc-related basalts, while the high-titanium basalts resemble ocean island basalts [37]. The erosion of the high-titanium basalts has contributed to the generation of Ti−rich placers in the eastern part of the ELIP (Figs. 5, 6) [37]. Several extensively studied gabbro intrusions in the ELIP, particularly linked to Fe−Ti−V oxide mineralization, include the Panzhihua, Taihe, Baima, Hongge, and Xinjie intrusions (Figs. 5, 6) [38]. The Hongge and Xinjie intrusions exhibit ultramafic rocks that are mineralized with disseminated sulfides rich in nickel (Ni), copper (Cu), and platinum group elements (PGE) (Fig. 2) [37,38]. Geological data revealed that the ore fluid has a mantle source derived from the degassing of primary melts [38]. Due to the continuous subduction of the Indian Plate and its association with the activity of the mantle plume and the intrusion of basic and ultrabasic materials, the mineral deposit system is likely to be unique in the vicinity of ELIP. These mineral deposits in ELIP might derive from the upper mantle upwelling associated with the continuous collision of the Indian Plate. On the other hand, Tengchong volcanic had a large-scale eruption in the late Paleozoic period. The geochemical properties of the original magma, such as high magnesium content, suggest that the mineral deposits were likely formed from the intrusion of basic and ultrabasic mantle source materials into the crust [37−39].

4.3 Dynamic model

The intrusion of ultrabasic materials into the crust can form mineral deposits. It was generally considered that the precipitation of minerals from fluids was released during the magma's solidification [40]. These fluids are rich in metal ions, which can precipitate to form metallic mineral deposits. Additionally, the high temperatures and pressures of the lower crust can cause metamorphism of the surrounding rocks, resulting in the formation of new minerals. The location and concentration of the mineral deposit in the Yunnan Province are likely formed by the ultrabasic mantle source materials associated with asthenospheric upwelling [37,38]. The low-velocity anomalies are widely distributed in the lower crust around the southeastern margin of the Tibetan Plateau, which was interpreted as partially molten material in the lower crust and upper mantle [27]. However, the low-velocity anomalies are surrounded by the

high-velocity anomaly, which might be considered a lithospheric barrier blocking the southeastward low crustal molten material flow. The lower crustal flow then converged near the relatively weak region at the interaction of the Xiaojiang fault, Lijiang−Xiaojinhe fault, and the north Red River fault [41−43]. Geological data show that large mineral deposits are spread in these convergence areas (Fig. 7) [44]. Then, this lower crustal flow might further promote the formation of mineral resources.

Three hypotheses for the formation of regional mineral deposits are then proposed: (1) The deep subduction of the Indian continent caused the Tibetan lower crust to move eastward [28], resulting in the formation of the metamorphic rocks. This metamorphism also created heat-flow conduits, which allows metamorphic fluids to move through faults and crustal-scale shear zones as hydrothermal and epithermal fluids, leading to mineral migration and mineral deposits. (2) Due to a low-velocity layer in the lower crust, stress cannot be transmitted between the upper crust and upper mantle, resulting in a decoupling of deformation between the crust and upper mantle [44]. The lower crustal material might associate with the upper mantle upwelling [44] and gathering at the bottom of the crust via a heat flow. Meanwhile, partial melting of the metasomatized lithospheric mantle can provide a well-linked architecture for transporting the mineral-rich melts and fluids in the crustal-scale shear zone, forming large-volume mineralized zones. (3) Due to the collision of the Indian and Eurasian plates, a large magmatic system has been formed, resulting in large volumes of magma. When magma rose to the surface, it would cool and form a wide range of metallic minerals. Combined with the geological data and our observations, a new dynamic model for the formation of mineral resources is then proposed and drawn in Fig. 8.

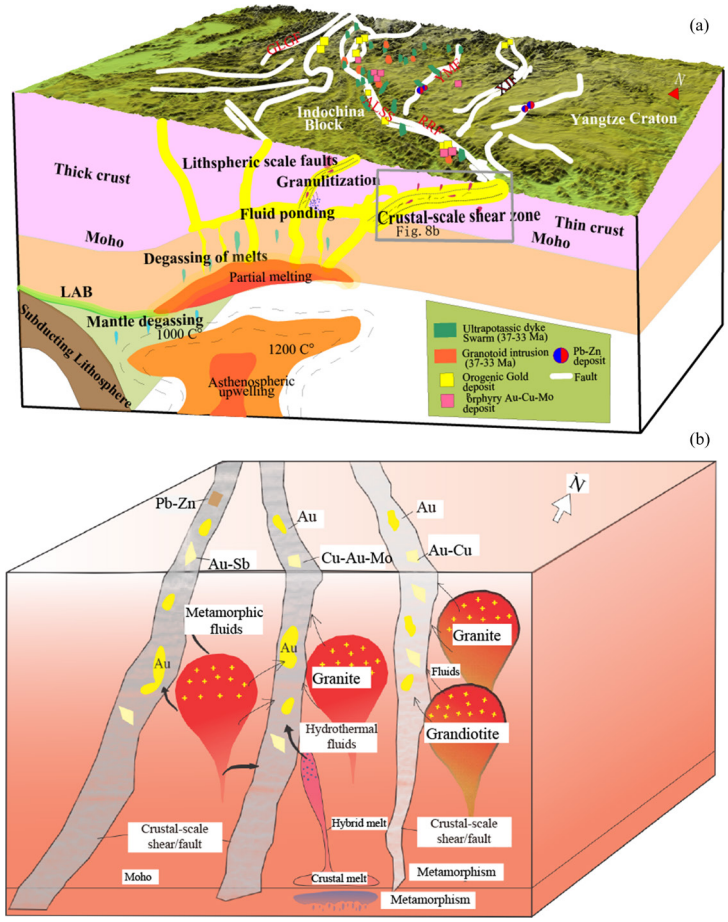

Fig. 8 (a) Dynamic model of mineral deposit formation associated with asthenospheric upwelling [44] and lower crustal flow [28]; (b) Hydrothermal activity and metallogenic environment on deep large fracture zones, enlarged from black rectangle in Fig. 8(a) (The white lines in (a) represent the regional faults; ALF: Ailaoshan fault; GLGF: Gaoligong fault; SGF: Sagaing fault; RRF: Red River fault; XJF: Xiaojiang fault; YMF: Yuanyuan−Muliou fault; LAB: Lithosphere−asthenosphere boundary [18])

5 Conclusions

(1) Shear wave velocity images are obtained using double-difference tomography in the Yunnan Province. The observed low-velocity zone mainly spread in the Lijiang-Xiaojinhe and Xiaojiang fault zones, which might relate to the low crustal flow. Emeishan Large Igneous Rock, with the high velocity has obstructed the low crustal flow.

(2) The relationship between the low-velocity zone and various metallic minerals was analyzed, and it is proposed that the metamorphic fluids have moved through faults and weak crust shear zones as hydrothermal and epithermal fluids, leading to mineral migration and deposit.

(3) A dynamic model for deep mineralization is built, which provides a new understanding of the relation between the mineral deposition system and the low crustal flow. It also significantly improves the mine exploration in Yunnan Province and its surroundings.

Acknowledgments

We thank the Data Management Center of the China Earthquake Administration for providing the waveform data for this study. This study is supported by the National Natural Science Foundation of China (Nos. 42274083, 41974049, 42074109).

References

[1] HOU Zeng-qian, YANG Zhi-ming, LU Yong-jun, KEMP A, ZHENG Yuan-chuan, LI Qiu-yun, DUAN Lian-feng. A genetic linkage between subduction- and collision-related porphyry Cu deposits in continental collision zones [J]. Geology, 2015, 43(3): 247−250.

[2] ZOU Hao, LI Min, SANTOSH M, ZHENG Da, CAO Hua-wen, JIANG Xiu-wei, CHEN Hai-feng, LI Zhong-quan. Fault-controlled carbonate-hosted barite−fluorite mineral systems: The Shuanghe deposit, Yangtze Block, South China [J]. Gondwana Research, 2022, 101: 26−43.

[3] XU Lei-luo, BI Xian-wu, HU Rui-zhong, ZHANG Xin-chun, SU Wei-chao, QU Wen-jun, HU Zhao-chu, TANG Yong-yong. Relationships between porphyry Cu−Mo mineralization in the Jinshajiang–Red River metallogenic belt and tectonic activity: Constraints from zircon U−Pb and molybdenite Re−Os geochronology [J]. Ore Geology Reviews, 2012, 48: 460−473.

[4] WANG E, BURCHFIEL B C. Late Cenozoic to Holocene deformation in southwestern Sichuan and adjacent Yunnan, China, and its role in formation of the southeastern part of the Tibetan plateau [J]. Geological Society of America Bulletin, 2000, 112: 413−423.

[5] LIU Chuan-ming, YAO Hua-jian, YANG Hsin-ying, SHEN Wei-sen, FANG Hong-jian, HU Shao-qian, QIAO Lei. Direct inversion for three-dimensional shear wave speed azimuthal anisotropy based on surface wave ray tracing: Methodology and application to Yunnan, southwest China [J]. Journal of Geophysical Research: Solid Earth, 2019, 124(11): 11394−11413.

[6] ZHANG Zhi-qi, YAO Hua-jian, YANG Yan. Three-dimensional S-wave velocity structure and dynamic significance of mantle on the southeast margin of the Qinghai-Tibet Plateau [J]. Science China: Earth Sciences, 2020, 50(9): 219−225. (in Chinese)

[7] ZUO Ren-guang, XIONG Yi-hui, WANG Jian, CARRANZA E J M. Deep learning and its application in geochemical mapping [J]. Earth−Science Reviews, 2019, 192: 1−14.

[8] WU Teng-feng, ZHANG Shuang-xi, LI Meng-kui, QIN Wei-bing, ZHANG Chao-yu. Two crustal flowing channels and volcanic magma migration underneath the SE margin of the Tibetan Plateau as revealed by surface wave tomography [J]. Journal of Asian Earth Sciences, 2016,132: 25−39.

[9] LIU Bang-jun, SPIEKERMANN R, ZHAO Cun-liang, PÜTTMANN W, SUN Yu-zhuang, JASPER A J, UHL D. Evidence for the repeated occurrence of wildfires in an upper Pliocene lignite deposit from Yunnan, SW China [J]. International Journal of Coal Geology, 2022, 250: 103924.

[10] WEI Yue-hua, ZI Jian-wei, LIU Gui-chun, SUN Zai-bo, CHEN Guang-yan, ZHAO Tian-yu, NIE Xiao-mei, YANG Zhao. Reconstructing the Lancang Terrane (SW Yunnan) and implications for Early Paleozoic Proto-Tethys evolution at the northern margin of Gondwana [J]. Gondwana Research, 2022, 101: 278−294.

[11] CHENG Qiu-ming. Mapping singularities with stream sediment geochemical data for prediction of undiscovered mineral deposits in Gejiu, Yunnan Province, China [J]. Ore Geology Reviews, 2007, 32(1/2): 314−324.

[12] YAO Hua-jian, van der HILST R D, de HOOP M V. Surface-wave array tomography in SE Tibet from ambient seismic noise and two-station analysis—I: Phase velocity maps [J]. Geophysical Journal International, 2006, 166(2): 732−744.

[13] XU Yang-bao, QIN Wen-qing, LIU hui. Mineralogical characterization of tin-polymetallic ore occurred in Mengzi, Yunnan Province, China [J]. Transactions of Nonferrous Metals Society of China, 2012, 22(3): 725−730.

[14] BAO Xue-wei, SUN Xiao-xiao, XU Ming-jie, EATON D W, SONG Xiao-dong, WANG Liang-shu, WANG Pan. Two crustal low-velocity channels beneath SE Tibet were revealed by joint inversion of Rayleigh wave dispersion and receiver functions [J]. Earth and Planetary Science Letters, 2015, 415: 16−24.

[15] ZHENG Xiu-fen, YAO Zhi-xiang, LIANG Jiang-hong, ZHENG Jie. The role played and opportunities provided by IGP DMC of China National Seismic Network in Wenchuan earthquake disaster relief and researches [J]. Bulletin of the Seismological Society of America, 2010, 100(5B), 2866−2872.

[16] ZHANG Hai-jiang, THURBER C H. Double-difference tomography: The method and its application to the Hayward fault, California [J]. Bulletin of the Seismological Society of America, 2003, 93(5): 1875−1889.

[17] YAO Hua-jian. Building the community velocity model in the Sichuan Yunnan region, China: Strategies and progresses [J]. Science China: Earth Sciences, 2020, 63: 1425−1428. (in Chinese)

[18] LIU Ying, YAO Hua-jian, ZHANG Hai-jiang, FANG Hong-jian. The community velocity model V. 1.0 of southwest China, constructed from joint body- and surface-wave travel-time tomography [J]. Seismological Research Letters, 2021, 92(5): 2972−2987.

[19] LV Miao-miao, DING Zhi-feng, XU Xiao-ming. Seismogenic environments of earthquakes on the southeastern margin of the Tibetan Plateau revealed by double-difference tomography [J]. Tectonophysics, 2022, 843: 229603.

[20] LIU Wei, WU Qing-ju, ZHANG Feng-xue. Crustal structure of southeastern Tibetan Plateau inferred from double-difference tomography [J]. Acta Seismologica Sinica, 2019, 41(2): 155−168.

[21] DENG Shan-quan, ZHANG Wen-bo, YU Xiang-wei, SONG Qian, WANG Xiao-na. Analysis on crustal structure characteristics of southern Sichuan−Yunnan by regional double-difference seismic tomography [J]. Chinese Journal of Geophysics, 2020, 63(10): 3653−3668. (in Chinese)

[22] GUO Qing-hai, LIU Ming-liang, LI Jie-xiang, ZHANG Xiao-bo, GUO Wei, WANG Yan-xin. Fluid geochemical constraints on the heat source and reservoir temperature of the Banglazhang hydrothermal system, Yunnan-Tibet Geothermal Province, China [J]. Journal of Geochemical Exploration, 2017, 172: 109−119.

[23] ZHANG Chang-qing, WU Yue, HOU Lin, MAO Jing-wen. Geodynamic setting of mineralization of Mississippi Valley-type deposits in world-class Sichuan–Yunnan–Guizhou Zn−Pb triangle, southwest China: Implications from age-dating studies in the past decade and the Sm−Nd age of Jinshachang deposit [J]. Journal of Asian Earth Sciences, 2015, 103: 103−114.

[24] LIU Quan-you, ZHU Dong-ya, JIN Zhi-jun, LIU Chun-yan, ZHANG Dian-wei, HE Zhi-liang. Coupled alteration of hydrothermal fluids and thermal sulfate reduction (TSR) in ancient dolomite reservoirs — An example from Sinian Dengying Formation in Sichuan Basin, Southern China [J]. Precambrian Research, 2016, 285: 39−57.

[25] WANG Fan-yun, MAO Xian-cheng, DENG Hao, ZHANG Bao-yi. Manganese potential mapping in western Guangxi-southeastern Yunnan (China) via spatial analysis and modal-adaptive prospectivity modeling [J]. Transactions of Nonferrous Metals Society of China, 2020, 30(4): 1058−1070.

[26] LI Gong-Jian, WANG Qing-fei, HUANG Yu-han, GAO Lei, YU Li. Petrogenesis of Middle Ordovician peraluminous granites in the Baoshan block: Implications for the Early Paleozoic tectonic evolution along East Gondwana [J]. Lithos, 2016, 245: 76−92.

[27] YU Nian, UNSWORTH M, WANG Xu-ben, LI De-wei, WANG En-ci, LI Rui-heng, HU Yuan-bang, CAI Xue-lin. New insights into crustal and mantle flow beneath the red River Fault zone and adjacent areas on the southern margin of the Tibetan Plateau revealed by a 3-D magnetotelluric study [J]. Journal of Geophysical Research: Solid Earth, 2020, 125(10): e2020JB019396.

[28] SUN Ya, NIU Feng-lin, LIU Hua-feng, CHEN You-lin, LIU Jian-xin. Crustal structure and deformation of the SE Tibetan plateau revealed by receiver function data [J]. Earth and Planetary Science Letters, 2012, 349/350: 186−197.

[29] SUN Ya, LIU Jian-xin, ZHOU Ke-ping, CHEN Bo, GUO Rong-wen. Crustal structure and deformation under the Longmenshan and its surroundings revealed by receiver function data [J]. Physics of the Earth and Planetary Interiors, 2015, 244: 11−22.

[30] ZHANG Xiu-wu, YANG Lin-sheng, LI Yong-hua, LI Hai-rong, WANG Wu-yi, GE Quan-sheng. Estimation of lead and zinc emissions from mineral exploitation based on characteristics of lead/zinc deposits in China [J]. Transactions of Nonferrous Metals Society of China, 2011, 21(11): 2513−2519.

[31] ZHAO Lian-feng, XIE Xiao-bi, HE Jian-kun, TIAN Xiao-bo, YAO Zhen-xing. Crustal flow pattern beneath the Tibetan Plateau constrained by regional Lg-wave Q tomography [J]. Earth and Planetary Science Letters, 2013, 383: 113−122.

[32] WANG Cai-yan, HAN Run-sheng, HUANG Jian-guo, XU Sai-hua, REN Tao. The $^{40}Ar-^{39}Ar$ dating of biotite in ore veins and zircon U−Pb dating of porphyrtic granite dyke in the Nanyangtian tungsten deposit in SE Yunnan, China [J]. Ore Geology Reviews, 2019, 114: 103133.

[33] WANG Qing-fei, GROVES D I, DENG Jun, LI Hua-jian, YANG Lin, DONG Chao-yi. Evolution of the Miocene Ailaoshan orogenic gold deposits, southeastern Tibet, during a complex tectonic history of lithosphere-crust interaction [J]. Mineralium Deposita, 2020, 55: 1085−1104.

[34] HOU Zeng-qian, WANG Qing-fei, ZHANG Hai-jiang, XU Bo, YU Nian, WANG Rui. Lithosphere architecture characterized by crust-mantle decoupling controls the formation of orogenic gold deposits [J]. National Science Review, 2022, 10(3): nwac257.

[35] REN Yan-zong, LU Zhan-wu, ZHANG Xin-yan, XUE Shuai, WANG Guang-wen. Crustal structure of the Emeishan large igneous province inner zone is revealed by deep seismic reflection profile [J]. Chinese Journal of Geophysics, 2022, 65(2): 484−494. (in Chinese)

[36] LIU Yi-duo, LI Lun, van WIJK J, LI Ai-bing, FU Yuan-yuan V. Surface-wave tomography of the Emeishan large igneous Province (China): Magma storage system, hidden hotspot track, and its impact on the Capitanian mass extinction [J]. Geology, 2021, 49(9): 1032−1037.

[37] LI Ni, ZHAO Yong-wei, ZHANG Liu-yi, WANG Jia-long. The quaternary eruptive sequence of the Tengchong volcanic group, southwestern China [J]. Lithos, 2020, 354/355: 105173.

[38] MUNTEANU M, YAO Yong, WILSON A H, CHUNNETT G, LUO Yao-nan, HE Hong, CIOACA M, WEN Mao-lin. Panxi region (Southwest China): Tectonics, magmatism and metallogenesis: A review [J]. Tectonophysics, 2013, 608: 51−71.

[39] CHEN Jian-lin, XU Ji-feng, WANG Bao-di, YANG

Zhi-ming, REN Jiang-bo, YU Hong-xia, LIU Hong-fei, FENG Yue-xing. Geochemical differences between subduction-and collision-related copper-bearing porphyries and implications for metallogenesis [J]. Ore Geology Reviews, 2015, 70: 424−437.

[40] XU Yi-gang, ZHONG Sun-lin. Emei Mountain igneous rocky province: Evidence of mantle plume activity and its melting conditions [J]. Geochemistry, 2001, 1: 1−9.

[41] LIU Jian-xin, SHAHZAD M, SUN Ya, SHAHZAD A, LI Chuan, FANIDI M, MUHAMMAD I. Deep metallogenic mechanism in southeastern China based on receiver function data [J]. Transactions of Nonferrous Metals Society of China, 2022, 32(1): 273−284.

[42] SHAHZAD S M, LIU Jian-xin, SUN Ya, LI Chuan. Crustal structure and deformation in southeastern China revealed by receiver functions [J]. Journal of Asian Earth Sciences, 2021, 221: 104937.

[43] FU Yuan-yuan, GAO Yuan, LI Ai-bing, LI Lun, CHEN An-guo. Lithospheric structure of the southeastern margin of the Tibetan Plateau from Rayleigh wave tomography [J]. Journal of Geophysical Research: Solid Earth, 2017, 122(6): 4631−4644.

[44] CHEN Xiao-cui, HU Rui-zhong, BI Xian-wu, ZHONG Hong, LAN Jiang-bo, ZHAO Cheng-hai, ZHU Jing-jing. Zircon U−Pb ages and Hf−O isotopes, and whole-rock Sr−Nd isotopes of the Bozhushan granite, Yunnan Province, SW China: Constraints on petrogenesis and tectonic setting [J]. Journal of Asian Earth Sciences, 2015, 99: 57−71.

地震波成像揭示云南省的热液活动和成矿环境

孙 娅[1,2]，邓士林[1,2]，柳健新[1,2]，Syed Muzyan SHAHZAD[1,2]，陈 波[1,2]

1. 中南大学 地球科学与信息物理学院，长沙 410083；
2. 中南大学 有色资源与地质灾害探查湖南省重点实验室，长沙 410083

摘 要：采用双差定位层析成像方法揭示 S 波速度结构，显示大规模低速异常主要集中在 10~25 km 深度的小江断裂带和丽江−小金河断裂带周围；而在川滇块体中南部区域存在一个明显的高速异常，这与峨眉山大型火成岩省分布区域范围一致。根据地质和地球物理资料，推断小江断裂带和丽江−小金河断裂带下的低速异常与来自青藏高原中部的下地壳流动有关。然而，峨眉山地区中部存在明显的高速异常，与峨眉山大型火成岩区一致。峨眉山下方的与地幔柱相关高速异常会阻碍地壳流动，从而使得地壳流被限制在深大断裂带附近。结果还发现多种矿产资源主要集中在大型断层和低速带上，表明下地壳流动和大型深部断层为流体成矿和矿床沉积提供了条件。

关键词：云南省；地震波层析成像；下地壳流；成矿环境

(Edited by Xiang-qun LI)